*processes*

*Article*

# 3D Printing of PLA/Magnetic Ferrite Composites: Effect of Filler Particles on Magnetic Properties of Filament

**Abdulkarim Amirov [1,*], Alexander Omelyanchik [1], Dmitry Murzin [1], Valeria Kolesnikova [1], Stanislav Vorontsov [1], Ismel Musov [2], Khasan Musov [2], Svetlana Khashirova [2] and Valeria Rodionova [1]**

1 Research and Education Center "Smart Materials and Biomedical Applications", Immanuel Kant Baltic Federal University, 236014 Kaliningrad, Russia
2 Progressive Materials and Additive Technologies Center, Kabardino-Balkarian State University Named after H.M. Berbekov, 360004 Nalchik, Russia
* Correspondence: amiroff_a@mail.ru

**Abstract:** Three-dimensional printing is one of the most promising areas of additive manufacturing with a constantly growing range of applications. One of the current tasks is the development of new functional materials that would allow the manufacture of objects with defined magnetic, electrical, and other properties. In this work, composite magnetic filaments for 3D printing with tunable magnetic properties were produced from polylactic acid thermoplastic polymer with the addition of magnetic ferrite particles of different size and chemical composition. The used magnetic particles were cobalt ferrite $CoFe_2O_4$ nanoparticles, a mixture of $CoFe_2O_4$ and zinc-substituted cobalt ferrite $Zn_{0.3}Co_{0.7}Fe_2O_4$ nanoparticles (~20 nm), and barium hexaferrite $BaFe_{12}O_{19}$ microparticles (<40 µm). The maximum coercivity field $H_C$ = 1.6 ± 0.1 kOe was found for the filament sample with the inclusion of 5 wt.% barium hexaferrite microparticles, and the minimum $H_C$ was for a filament with a mixture of cobalt and zinc–cobalt spinel ferrites. Capabilities of the FDM 3D printing method to produce parts having simple (ring) and complex geometric shapes (honeycomb structures) with the magnetic composite filament were demonstrated.

**Keywords:** magnetic nanoparticles; spinel ferrites; hexaferrites; polymer composites; magnetic composites; additive technologies; filament; extrusion; FDM printing

check for updates

**Citation:** Amirov, A.; Omelyanchik, A.; Murzin, D.; Kolesnikova, V.; Vorontsov, S.; Musov, I.; Musov, K.; Khashirova, S.; Rodionova, V. 3D Printing of PLA/Magnetic Ferrite Composites: Effect of Filler Particles on Magnetic Properties of Filament. *Processes* **2022**, *10*, 2412. https://doi.org/10.3390/pr10112412

Academic Editor: Tizazu Mekonnen

Received: 20 October 2022
Accepted: 11 November 2022
Published: 16 November 2022



## 1. Introduction

Three-dimensional printing technology has been growing with an impressive speed over the past few years; it offers an economical use of resources (raw material), as well as a wide range of possibilities for varying geometric shapes and functional properties of printed objects [1–3]. Among the methods related to additive manufacturing technologies, the simplest and the most common is the FDM (fused deposition melting) method also known as FFF (fused filament fabrication), in which a 3D object is created via layer-by-layer extrusion of a thermoplastic polymer [4]. This method is one of the most promising for the 3D printing of composites with various additives to extend the functionality of the material [5,6]. The types of additives depend on the required final parameters for a product and require the development of new technologies to produce composite filaments suitable for the FDM printing method.

A common and the most readily available filament used for FDM printing is polylactide (PLA), whose monomer is lactic acid. PLA is biodegradable, biocompatible, and thermoplastic, which makes it promising for use in biomedical applications [7]. Currently available filaments for FDM printing are limited to commercially available polymeric plastics (e.g., PLA, ABS, HIPS, and BFlex) and their modifications. However, composite filaments based on polymers with metallic additives, which have increased mechanical strength and provide magnetic properties, are presented on the market in limited quantities [8]. On the other hand, an important challenge is to obtain a composite filament with additives of magnetic particles having specific functional characteristics (giant magnetostriction, magnetic anisotropy, and selective absorption of electromagnetic waves), which allows printing objects for narrowly focused practical applications [9–11]. Such fillers providing materials with functional properties can be magnetic nano- and microparticles [12]. Opportunities that are enabled by the 3D printing of magnetic materials are huge due to the possibility of fabricating objects with predetermined magnetic properties (soft or hard magnetic) that can be controlled, e.g., by the inclusion of certain fillers [13]. This will allow complex geometric structures with certain magnetic properties to be manufactured for applications in electronics, sensors, soft robotics, biomedicine, etc. [14–20].

Among magnetic materials, spinel ferrites and hexaferrites (oxides based on transition metals that can be obtained in the form of nano- and microparticles) are of particular interest because of their chemical stability, as well as good mechanical, strong magnetic, and tunable electrical properties [21]. Cobalt ferrite has the highest magnetocrystalline anisotropy value ($2 \times 10^6$ erg/cm$^3$ [22]) among spinel ferrites. It has been shown that a small content of zinc in the structure of cobalt ferrite increases the saturation magnetization, but the coercivity associated with the magnetic anisotropy decreases [23–25]. Hexaferrites, such as barium hexaferrite, have a large magnetocrystalline anisotropy constant ($3.3 \times 10^6$ erg/cm$^3$ [26]), but they are difficult to produce in the form of nanoparticles because of the need for high-temperature annealing and quite complicated synthesis method [27,28]. Thus, magnetic properties of particles depend on structure, chemical composition, particle size, and other factors that can be tuned during the particle synthesis to meet the requirements of a target application. In this study, we implemented two synthesis approaches to produce magnetic particles: a top-down approach of ball milling to obtain barium hexaferrite microparticles and a bottom-up sol–gel chemical synthesis of spinel ferrite nanoparticles [28–30]. Nanoparticles are preferable for composites because they can be easily homogeneously distributed in the polymer matrix, thereby minimizing disturbance of the polymer structure; however, with the decrease in size, magnetic properties degrade due to the increasing fraction of the surface characterized by a magnetic disorder [31,32].

This work aims to develop the technology for the fabrication of filament composite based on PLA with the inclusion of ferrite particles with various magnetic properties and sizes, namely, cobalt ferrite nanoparticles, a mixture of pure and zinc-substituted cobalt ferrite particles, and barium hexaferrite microparticles. The magnetic properties of the produced filaments were studied, and the possibility to use these filaments for 3D printing was demonstrated.

## 2. Materials and Methods

### *2.1. Filler Particles*

Three types of fitter particles were used to produce composite filaments:

(1) Cobalt ferrite $CoFe_2O_4$ (CFO);
(2) Mixture (1:1) of $CoFe_2O_4$ and zinc-substituted cobalt ferrite $Zn_{0.3}Co_{0.7}Fe_2O_4$ (CFO/ZCFO);
(3) Barium hexaferrite $BaFe_{12}O_{19}$ (BaFO).

Magnetic $CoFe_2O_4$ and $Zn_{0.3}Co_{0.7}Fe_2O_4$ nanoparticles with a spinel ferrite crystal structure were synthesized using the sol–gel self-combustion approach [29]. For this, $Zn(NO_3)_2{\cdot}6H_2O$ (≥98%; LenReactiv, St. Petersburg, Russia), $Co(NO_3)_2{\cdot}6H_2O$ (>98%; Vekton, St. Petersburg, Russia), and $Fe(NO_3)_3{\cdot}6H_2O$ (≥98%; LenReactiv, St. Petersburg, Russia), aqueous ammonia solution ($NH_3$(aq) > 25%; SIGMATEK LLC, Khimki, Russia), citric acid $C_6H_8O_7{\cdot}H_2O$ (≥99.8%; LenReactiv, St. Petersburg, Russia), and distilled water were used. The metal salts were taken in the molar ratio of cations $Co^{2+}$:$Fe^{3+}$ = 1:2 and $Zn^{2+}$:$Co^{2+}$:$Fe^{3+}$ = 0.3:0.7:2 to maintain the stoichiometry of $CoFe_2O_4$ and $Zn_{0.3}Co_{0.7}Fe_2O_4$, respectively. In atypical synthesis, 1 M citric acid solution was added to 1 M aqueous solutions of metal nitrates of the same volume. The pH was adjusted by adding aqueous ammonia until a neutral level of ~7 was reached. The resulting solutions were left on a heating plate at 150 °C and stirred vigorously until the gel was reached. The nanopowders were obtained by increasing the temperature to 300 °C, thus initiating a self-combustion reaction. The reaction product was ground in an agate mortar and washed several times with distilled water and acetone. The average size of the obtained crystallites did not exceed 20 nm. A detailed characterization of magnetic and structural properties of the nanopowders is described in [24].

BaFO microparticles were obtained by the ball milling of the commercial barium hexaferrite permanent magnet. The preliminarily demagnetized sample of barium hexaferrite in the form of a cylinder was crushed to large granules with the average diameter of 3 mm and then ground in the agate mortar to a fine-grained powder. The resulting powder was then milled in the ball mill (E-Max, Retsch GmbH, Haan, Germany) in two stages for 1.5 h (stage I) and 30 min (stage II) with the addition of isopropyl alcohol (~25 mL) at 500 rpm. The resulting powder was dried and sieved using a 40 μm sieve after the first and the second stages. The resulting powder was dried at 80 °C for 12 h.

### *2.2. Fabrication of Filaments*

A tabletop Twin Tech Screw extruder (TwinTech Extrusion, Ltd., Stoke-on-Trent, UK) with five heating zones was used to produce the filament composite. Printing of test objects from a composite filament was performed using a 3D FDM printer AnyCYBIC Mega-S (Shenzhen Anycubic Technology Co., Ltd., Guangdong, China). Figure 1 shows the process flowchart of a composite filament fabrication with magnetic additives for FDM printing. The protocol for obtaining a magnetic composite filament for FDM printing consisted of the sequential steps described below.

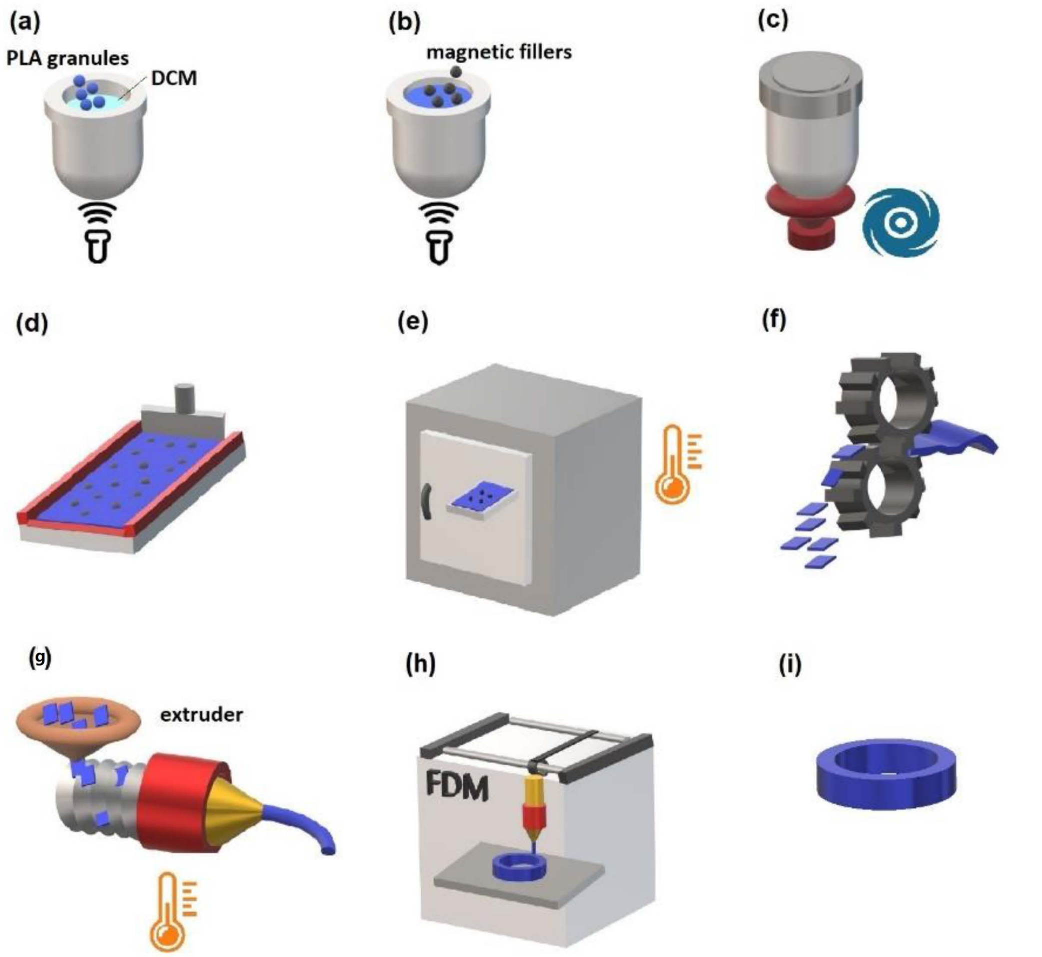


**Figure 1.** Schematic representation of a PLA-based composite magnetic filament preparation for FDM printing: (**a**) preparation of the PLA solution; (**b**) filler addition; (**c**) homogenization; (**d**) composite film preparation; (**e**) drying; (**f**) pelletizing; (**g**) extrusion; (**h**) FDM printing of the object; (**i**) final object.

1. *Preparation of the PLA solution (Figure 1a)*

At this stage, PLA pellets were cut from the filament and dried in a drying oven for 12 h at 40 °C to remove excess moisture. Then, PLA pellets were diluted in methylene chloride (DCM) in the mass ratio of 1:20. Complete dissolution of the PLA and obtention of a homogeneous solution were achieved by placing the solution in an ultrasonic bath for 90 min at room temperature with intermediate mechanical mixing using a glass rod.

2. *Adding the filler (Figure 1b)*

Next, magnetic particles were added to the prepared PLA solution and mixed for at least 60 min using an ultrasonic bath. The calculated mass fraction of the magnetic additives was 5% and 10% of the composite total mass. Table 1 shows the composition and concentrations of the magnetic filler particles used in the preparation of composite filaments.

**Table 1.** Types and concentrations of magnetic particle fillers in composite filaments.

| Type of Fillers | Mass Fraction, % | Designation |
|---|---|---|
| CFO | 5 | 5CFO/PLA |
| CFO | 10 | 10CFO/PLA |
| CFO/ZCFO | 5 | 5CFO/ZCFO/PLA |
| BaFO | 5 | 5BaFO/PLA |

3. *Homogenization (Figure 1c)*

The obtained PLA solutions with the magnetic particles were mixed before the final pouring using a vortex mixer.

4. *Composite film preparation (Figure 1d)*

Composite films were obtained via solvent casting assisted by a doctor blade technique to control the film thickness. The resulting solution was poured onto a glass mold and smoothed with a sharp blade to obtain homogeneous composite films [33,34].

5. *Drying (Figure 1e)*

In this step, composites were prepared by evaporating the solvent in an oven at the temperature of 30 °C for 60 min. It should be noted that the boiling temperature of DCM solvent is about 40 °C, and the selected drying protocol contributed to decreasing the sedimentation of the magnetic fillers, due to faster evaporation than at room temperature and an increase in the viscosity of the basic solution. The final drying took place for 12 h at room temperature in a fume hood. The thickness of the samples obtained after final drying was about 0.4 mm.

6. *Pelletizing (Figure 1f)*

The obtained composite sheets were cut into 5 mm wide thin strips and mechanically crushed using a granulator. The obtained composite flakes had an average linear size of about $3 \times 4 \times 1$ mm.

7. *Extrusion (Figure 1g)*

The obtained pellets were extruded into the composite filament at 185 °C. The rotation speed of the extruder was 15 rpm. The extruded composite filament was cooled in the air at room temperature. The filament diameter was studied with a laser thickness gauge. The diameter of a nozzle used for the extrusion process was about 1.78 mm.

8. *FDM printing of the objects (Figure 1h)*

Digital 3D models of test objects were made using the Autodesk Fusion 360 platform (Autodesk, Inc., San Francisco, CA, USA). The slicing of 3D models for 3D printing was performed with Cura 3D slicer software (Ultimaker B.V., Utrecht, The Netherlands), which slices a 3D model into layers and creates a G-code file for a 3D printer.

### 2.3. Characterization of Structural and Magnetic Properties of Samples

Magnetic properties of the composite filament samples were studied using a LakeShore 7400 vibrating magnetometer (Lake Shore Cryotronics, Inc., Westerville, OH, USA) at room temperature (~295 K). The measurements were performed on segments of the filament with a length of about 4 mm fixed perpendicularly to the magnetic field lines.

High-resolution X-ray computed tomography (XCT) YXLON (Cheetah, Hamburg, Germany) was used to visualize the internal microstructure of printed objects with a spatial resolution of no less than 1 μm.

## 3. Results and Discussion

### 3.1. Characterization of the Filaments

Figure 2 shows a picture of the CFO/PLA magnetic composite filament with a 10 wt.% concentration of cobalt ferrite filler. One of the main physical parameters of the filament, required for the FDM printing, is its diameter, which was determined during the extrusion process with a laser thickness gauge. The average filament diameter was 1.75 mm. For all composite filament samples, control measurements were performed on the 1 m filament length; the deviation of the diameter from the average value did not exceed ±0.05 mm.

**Figure 2.** Photo of the 10CFO/PLA magnetic composite filament.

It was found that the optimal concentration of the magnetic additives, required to obtain the homogeneous filament with minimal diameter deviation, was below 10%. A further increase in the concentration led to the significant diameter deviation of the filament (±0.25 mm) from the standard value due to the heterogeneity of the melted flow in the extruder.

### 3.2. Magnetic Properties

Magnetic hysteresis loops for all magnetic filament samples are plotted in Figure 3. All studied samples exhibit ferromagnetic behavior with significant coercive force ($H_C$) and magnetization ($M$) values. Since the maximum field of 12 kOe that could be generated with the used magnetometer was not sufficient to saturate the sample, the saturation magnetization ($M_S$) was obtained by extrapolating the $M$–$H$ curves with the following function:

$$M(H) = M_S \times \left(1 - \frac{A}{H} - \frac{B}{H^2}\right), \quad (1)$$

where $A$ and $B$ are free parameters related to the magnetic anisotropy of the particles [25,35]. Using Equation (1), a fitting of the $M$–$H$ dependencies in the range of magnetic 8–12 kOe was performed. The resulting $M_S$ values are reported in Table 1.

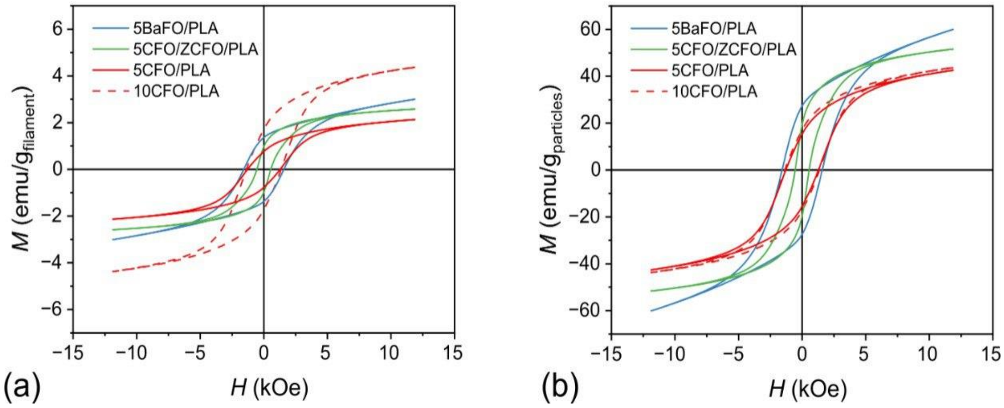


**Figure 3.** Room-temperature field-dependent magnetization curves measured for all samples of magnetic filaments. The magnetization is normalized to (**a**) the mass of the filament, and (**b**) the nominal content of the magnetic filler.

Measured magnetic characteristics of the composites are given in Table 2. The $M$ values were normalized to the filament's masses and corresponding masses of the magnetic inclusions. The magnetization value of a filament is proportional to the mass content of the magnetic inclusions. According to measurements, the maximum value $M_S$ = 5.4 ± 0.5 emu/g(filament) was achieved for the sample with the maximum concentration of magnetic particles 10CFO/PLA. However, from the samples with the same concentration of the magnetic nanoparticles, the sample with the inclusion of the barium hexaferrite microparticles 5BaFO/PLA showed a maximal $M_S$ value of 4.3 ± 0.4 emu/g(filament). In samples with ZCFO and CFO nanoparticles, this parameter decreased due to the increase in the fraction of surface atoms [31]. The saturation magnetization ~53–54 emu/g (particles) of CFO particles was slightly lower compared with $M_S$ = 69 ± 2 emu/g of CFO particles prepared using the same method [24].

**Table 2.** Magnetic properties of the filament measured at room temperature: magnetization measured in the 12 kOe field ($M_{12kOe}$); saturation magnetization was obtained by extrapolation of the $M$–$H$ dependences ($M_S$), residual magnetization ($M_R/M_S$), and coercivity field ($H_C$). The magnetization values were normalized to the mass of the filament and the mass of the particles contained in the filament according to the nominal particle concentration.

| Sample | $M_{12kOe}$ | | $M_S$ | | $M_R/M_S$ | $H_C$ |
|---|---|---|---|---|---|---|
| | emu/g$_{filament}$ | emu/g$_{particles}$ | emu/g$_{filament}$ | emu/g$_{particles}$ | % | kOe |
| 5CFO/PLA | 2.1 ± 0.2 | 43 ± 4 | 2.7 ± 0.3 | 53 ± 5 | 29 ± 5 | 1.3 ± 0.1 |
| 10CFO/PLA | 4.4 ± 0.4 | 44 ± 4 | 5.4 ± 0.5 | 54 ± 5 | 32 ± 5 | 1.4 ± 0.1 |
| 5CFO/ZCFO/PLA | 2.6 ± 0.3 | 52 ± 5 | 3.0 ± 0.3 | 60 ± 6 | 32 ± 5 | 0.55 ± 0.02 |
| 5BaFO/PLA | 3.0 ± 0.3 | 60 ± 6 | 4.3 ± 0.4 | 85 ± 8 | 32 ± 5 | 1.6 ± 0.1 |

The sample with zinc-substituted cobalt ferrite had a higher magnetization value but a lower coercivity value, which is in agreement with the behavior of nanoparticles with similar chemical composition [23–25]. Thus, the mixing of CFO and ZCFO particles made it possible to obtain a filament, on the one hand, with an increased value of saturation magnetization and, on the other hand, with a coercive field, which could be established simply by selecting the ratio between the hard and soft fractions. The 1:1 ratio chosen in this work allowed us to increase the saturation magnetization from 2.1 ± 0.2 to 2.6 ± 0.3 emu/g and reduce the coercivity by about half. The residual magnetization ($M_R/M_S$) for all the samples was on the order of 30%, which is lower than the expected value for noninteracting single-domain particles according to the Stoner–Wohlfarth model [36]. The maximum value of the coercivity field $H_C$ = 1.6 ± 0.1 kOe was found for the sample with the inclusion of the barium hexaferrite microparticles, and the minimum value was found for the sample with a mixture of cobalt and zinc–cobalt ferrites, as expected according to the bulk magnetocrystalline anisotropy of these materials [22,26].

### 3.3. 3D Printing

One of the main problems in FDM printing using a composite filament with magnetic fillers is nozzle clogging, irregular flow, and particles sticking to parts with residual magnetization, which ultimately leads to a poor print quality and printing of parts with imperfect geometric dimensions relative to the original digital model [37]. To demonstrate the FDM printing capabilities of the obtained composite filament, samples with magnetic additives and 3D printer with the nozzle diameter of 0.4 mm were used. For adjustment of the printing parameters, the original PLA filament with the declared printing temperature of 205–235 °C was used. The presence of the magnetic fillers in the composite led to small deviations in the extrusion speed and melting temperature compared to the original filament. Thus, the extruder and stage temperatures, filament flow rate in the extruder, fill format, and other parameters were selected during the printing process to prevent clogging of the 3D printer's extruder. The extruder and bed temperatures suitable for printing with the composite filaments were 235 °C and 40 °C, respectively.

In [38], PLA filament with additives of spherical steel microparticles with a concentration 5–12 vol.% (26–47 wt.%) was obtained. It was found that the printing temperature of the composite filament to produce parts with the optimal resolution was 170 °C, which is lower than for the original PLA (~215 °C). The addition of metallic particles increased the heat transfer of the composite filament, making it more fluid than the original PLA filament at the same printing temperature. The effect of the spherical metal microparticle additive concentration on mechanical and rheological properties of the filament was examined in [39]. It was found that the concentration increase of additives above 30% mass fraction led to a significant decrease in the mechanical properties of the filament and the dynamic viscosity of its melt. For the samples considered in this work, the optimal printing mode was within the limits stated by the manufacturer for the original PLA filament. This is because the used ferrite additives had worse thermal conductivity compared to metallic steel additives, and the selected concentration of magnetic additives (5 and 10 wt.%) did not lead to a significant change in the rheological properties of the molten filament with the same printing parameters as for pure PLA.

Figure 4 shows pictures of the objects printed using the FDM method with the pure and composite filament based on PLA with 5 wt.% of magnetic fillers. The quality of objects printed from the filament with 5 wt.% of fillers did not depend on the type of used particles. The same printing parameters were used for all printed objects of different geometric shapes: ring and honeycomb structures with the edge of the hexagon of about 2 mm.

The correspondence of the geometric shapes of the printed objects was checked by analyzing the optical images using the ImageJ software [40,41]. The outer ($D$) and inner ($d$) diameters of the rings were measured using the freehand tool, thus obtaining the major and minor diameters, as well as the perimeter ($P$) and surface area ($A$), of the circle. All measured parameters are given in Table 3.

**Table 3.** Geometrical parameters of printed rings: $D$ and $d$ are the diameters of the outer and inner circles, $AR$ is the aspect ratio, and $c$ is the circularity index.

| Sample | Outer Circle | | | Inner Circle | | |
|---|---|---|---|---|---|---|
| | $D$, cm | $AR$ | $c$ | $d$, cm | $AR$ | $c$ |
| PLA | $1.66 \pm 0.01$ | 1.01 | 0.917 | 0.99 * | 1.00 | 0.935 |
| 5CFO/PLA | $1.67 \pm 0.03$ | 1.03 | 0.919 | $0.98 \pm 0.01$ | 1.03 | 0.883 |
| 5CFO/ZCFO/PLA | $1.64 \pm 0.02$ | 1.03 | 0.897 | $1.00 \pm 0.02$ | 1.05 | 0.910 |
| 5BaFO/PLA | $1.65 \pm 0.02$ | 1.03 | 0.823 | $1.00 \pm 0.01$ | 1.03 | 0.941 |

* Deviation of the major and minor diameters for this value was less than the given significant digits.

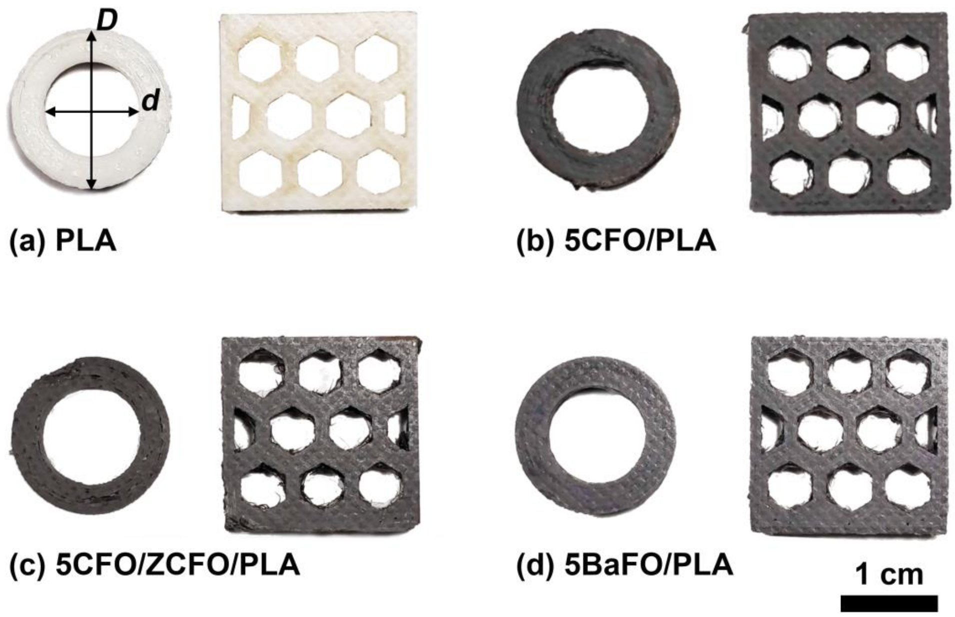


**Figure 4.** Pictures of objects printed with a 3D printer from the pure and composite PLA-based filament: (**a**) pure PLA; (**b**) 5CFO/PLA, (**c**) 5CFO/ZCFO/PLA, and (**d**) 5BaFO/PLA composites.

The error of the measured diameter was defined as the deviation between major and minor values. The aspect ratio ($AR$) parameter was defined as

$$AR = major/minor. \tag{2}$$

The correspondence of the printed objects to the perfect circle was checked by comparing the circularity ($c$) [40]:

$$c = 2\pi \cdot \frac{A}{p^2}. \tag{3}$$

For an ideal circle, $AR$ = 1 and $c$ = 0.913 are expected. For all printed objects with magnetic filler, a ~3% increase in the $AR$ parameter and a deviation of $c$ from the ideal value were observed. The highest deviation of $c$ of about 11% was found for the 5BaFO/PLA sample, while, for the remaining samples, this value does not exceed 3%. The PLA sample corresponded best to the specified parameters, but the deviations from the specified shapes of the printed magnetic nanocomposites were insignificant.

Standard characterization methods do not allow to study the internal structure of a printed object without its destruction, which was the motivation for using XCT. The internal microstructure was investigated using 3D XCT, and the results are shown in Figure 5. The XCT slices for printed pure PLA samples and its composites with 5 wt.% concentration of fillers helped us to determine that the quality of filling decreased for composite objects, which was noticeable due to gaps between the printed inner parts of the ring-shaped objects. However, such deterioration is not critical for printing with a composite filament with a selected filler concentration. The *Cura 3D* slicer allows the use of various filling patterns, the choice of which is determined by the required filling density in printing and the mechanical properties (e.g., bending strength) of the printed objects. For our printed objects, a cross-type pattern was used, which allows printing objects with a high filling.

As can be noticed, the composite filament led to a slight degradation of the internal microstructure, which was due to a change in the viscosity of the extruded flow, its variable speed, and the rapid curing resulting from the presence of magnetic additives.

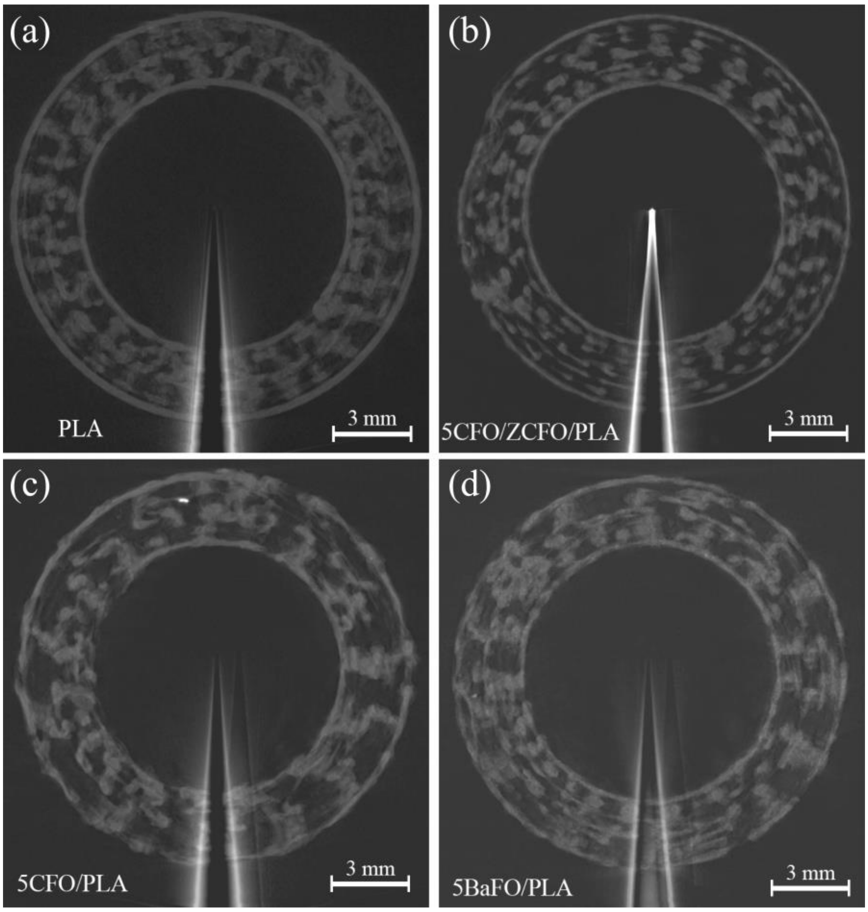


**Figure 5.** XCT slices of ring-shaped objects printed from pure (**a**) and composite filament (**b**–**d**).

## 4. Conclusions

This study demonstrated the possibilities of the 3D printing of ferrite-containing PLA objects using the FDM method. Magnetic properties of the filler particles could be finely tuned by the choice of synthesis approach and chemical engineering. Fabricated composite filaments possessed magnetic properties, which corresponded to those of filler particles; higher values of saturation magnetization and coercivity were found in the sample containing ball-milled barium hexaferrite microparticles. The quality of printed objects from composite filaments with a concentration of magnetic additives of 5 wt.% did not significantly depend on the type of particles used in the process. The diameter variation of the composite filament with 5–10 wt.% of ferrite filler after extrusion did not exceed 0.05 mm, while, for higher concentrations, the diameter of the composite filament was heterogeneous and not suitable for 3D FDM printing. The proposed approach can be used as a basis for the development of 3D–5D printing technologies with magnetic composite materials having controlled magnetic anisotropy and spatial distribution of particles in a polymer matrix. Thus, depending on demands, samples with barium ferrite fillers can be used in applications where high coercivity and residual magnetization are required and soft ferrites for applications where high susceptibility are required. Further prospects for this approach are related to printing in an external magnetic field, where the magnetic field applied during printing will allow locally controlling the microstructure of the printed objects to improve their mechanical properties, as well as adding a number of new functionalities such as self-healing and shape-memory properties [42]. The 3D printing of magnetic parts with a specific magnetization can be used to create magnetically controlled gears, actuators, and robot parts [13,19].

**Author Contributions:** Conceptualization, A.A. and A.O.; methodology, A.A., A.O. and I.M.; validation, A.O. and D.M.; formal analysis, A.O., D.M. and A.A.; investigation, S.V., D.M., V.K., K.M. and I.M.; resources, V.R. and S.K.; data curation, A.O., A.A. and D.M.; writing—original draft preparation, A.A.; writing—review and editing, A.A., A.O. and D.M.; visualization, A.O. and D.M.; supervision, S.K. and V.R.; project administration, V.R.; funding acquisition, V.R. All authors have read and agreed to the published version of the manuscript.

**Funding:** The research was funded by the Russian Science Foundation under Project no. 21-72-30032.

**Data Availability Statement:** The data presented in this study are available on request from the corresponding author.

**Acknowledgments:** The authors are grateful to Vladimir Leitsin and Alexander Tovpinets from Immanuel Kant Baltic Federal University (Kaliningrad, Russia) for their contribution and help with XCT measurements. Furthermore, the authors are grateful to Vitaly Salnikov from Immanuel Kant Baltic Federal University (Kaliningrad, Russia) for help with sample preparation and magnetic measurements. A.A. Amirov acknowledges the Russian Federal Academic Leadership Program Priority 2030 at the Immanuel Kant Baltic Federal University (milling of hexaferrite microparticles).

**Conflicts of Interest:** The authors declare no conflict of interest.

## References

1. Shi, Y.; Yan, C.; Zhou, Y.; Wu, J.; Wang, Y.; Yu, S.; Chen, Y. Overview of additive manufacturing technology and materials. In *Materials for Additive Manufacturing*; Elsevier: Amsterdam, The Netherlands, 2021; pp. 1–8.
2. Mahamood, R.M.; Jen, T.C.; Akinlabi, S.A.; Hassan, S.; Abdulrahman, K.O.; Akinlabi, E.T. Role of additive manufacturing in the era of Industry 4.0. In *Additive Manufacturing*; Elsevier: Amsterdam, The Netherlands, 2021; pp. 107–126.
3. Mondal, K.; Tripathy, P.K. Preparation of Smart Materials by Additive Manufacturing Technologies: A Review. *Materials* **2021**, *14*, 6442. [CrossRef] [PubMed]
4. Kristiawan, R.B.; Imaduddin, F.; Ariawan, D.; Ubaidillah; Arifin, Z. A review on the fused deposition modeling (FDM) 3D printing: Filament processing, materials, and printing parameters. *Open Eng.* **2021**, *11*, 639–649. [CrossRef]
5. Angelopoulos, P.M.; Samouhos, M.; Taxiarchou, M. Functional fillers in composite filaments for fused filament fabrication; A review. *Mater. Today Proc.* **2021**, *37*, 4031–4043. [CrossRef]
6. Wang, X.; Jiang, M.; Zhou, Z.; Gou, J.; Hui, D. 3D printing of polymer matrix composites: A review and prospective. *Compos. Part B Eng.* **2017**, *110*, 442–458. [CrossRef]
7. Giammona, G.; Craparo, E. Biomedical Applications of Polylactide (PLA) and Its Copolymers. *Molecules* **2018**, *23*, 980. [CrossRef]
8. Iron-Filled Metal Composite PLA, (n.d.). Available online: www.proto-pasta.com/products/magnetic-iron-pla (accessed on 1 September 2022).
9. Patton, M.V.; Ryan, P.; Calascione, T.; Fischer, N.; Morgenstern, A.; Stenger, N.; Nelson-Cheeseman, B.B. Manipulating magnetic anisotropy in fused filament fabricated parts via macroscopic shape, mesoscopic infill orientation, and infill percentage. *Addit. Manuf.* **2019**, *27*, 482–488. [CrossRef]
10. Taylor, A.P.; Velez Cuervo, C.; Arnold, D.P.; Velasquez-Garcia, L.F. Fully 3D-Printed, Monolithic, Mini Magnetic Actuators for Low-Cost, Compact Systems. *J. Microelectromechanical Syst.* **2019**, *28*, 481–493. [CrossRef]
11. Magisetty, R.; Cheekuramelli, N.S. Additive manufacturing technology empowered complex electromechanical energy conversion devices and transformers. *Appl. Mater. Today* **2019**, *14*, 35–50. [CrossRef]
12. Zhang, C.; Li, X.; Jiang, L.; Tang, D.; Xu, H.; Zhao, P.; Fu, J.; Zhou, Q.; Chen, Y. 3D Printing of Functional Magnetic Materials: From Design to Applications. *Adv. Funct. Mater.* **2021**, *31*, 2102777. [CrossRef]
13. Chatzipirpiridis, G.; Gervasoni, S.; Fischer, C.; Ergeneman, O.; Pellicer, E.; Nelson, B.J.; Pané, S. 3D Printing of Thermoplastic-Bonded Soft- and Hard-Magnetic Composites: Magnetically Tuneable Architectures and Functional Devices. *Adv. Intell. Syst.* **2019**, *1*, 1900069. [CrossRef]
14. Huber, C.; Abert, C.; Bruckner, F.; Groenefeld, M.; Schuschnigg, S.; Teliban, I.; Vogler, C.; Wautischer, G.; Windl, R.; Suess, D. 3D Printing of Polymer-Bonded Rare-Earth Magnets with a Variable Magnetic Compound Fraction for a Predefined Stray Field. *Sci. Rep.* **2017**, *7*, 9419. [CrossRef] [PubMed]

15. Hanemann, T.; Syperek, D.; Nötzel, D. 3D printing of ABS barium ferrite composites. *Materials* **2020**, *13*, 1481. [CrossRef] [PubMed]
16. Huber, C.; Cano, S.; Teliban, I.; Schuschnigg, S.; Groenefeld, M.; Suess, D. Polymer-bonded anisotropic SrFe12O19 filaments for fused filament fabrication. *J. Appl. Phys.* **2020**, *127*, 063904. [CrossRef]
17. Wei, X.; Liu, Y.; Zhao, D.; Mao, X.; Jiang, W.; Ge, S.S. Net-shaped barium and strontium ferrites by 3D printing with enhanced magnetic performance from milled powders. *J. Magn. Magn. Mater.* **2020**, *493*, 165664. [CrossRef]
18. Huber, C.; Goertler, M.; Abert, C.; Bruckner, F.; Groenefeld, M.; Teliban, I.; Suess, D. Additive Manufactured and Topology Optimized Passive Shimming Elements for Permanent Magnetic Systems. *Sci. Rep.* **2018**, *8*, 14651. [CrossRef]
19. Kim, Y.; Yuk, H.; Zhao, R.; Chester, S.A.; Zhao, X. Printing ferromagnetic domains for untethered fast-transforming soft materials. *Nature* **2018**, *558*, 274–279. [CrossRef]
20. Alapan, Y.; Karacakol, A.C.; Guzelhan, S.N.; Isik, I.; Sitti, M. Reprogrammable shape morphing of magnetic soft machines. *Sci. Adv.* **2020**, *6*, eabc6414. [CrossRef]
21. Varvaro, G.; Omelyanchik, A.; Peddis, D. Ferroic Transition Metal Oxide Nano-heterostructures: From Fundamentals to Applications. In *Tailored Functional Oxide Nanomaterials*; Wiley: Hoboken, NJ, USA, 2022; pp. 405–437.
22. Cullity, B.D.; Graham, C.D. *Introduction to Magnetic Materials*; John Wiley & Sons, Inc.: Hoboken, NJ, USA, 2008; Volume 12, ISBN 9780470386323.
23. Andersen, H.L.; Granados-Miralles, C.; Saura-Múzquiz, M.; Stingaciu, M.; Larsen, J.; Søndergaard-Pedersen, F.; Ahlburg, J.V.; Keller, L.; Frandsen, C.; Christensen, M. Enhanced intrinsic saturation magnetization of $Zn_xCo_{1-x}Fe_2O_4$ nanocrystallites with metastable spinel inversion. *Mater. Chem. Front.* **2019**, *3*, 668–679. [CrossRef]
24. Omelyanchik, A.; Levada, K.; Pshenichnikov, S.; Abdolrahim, M.; Baricic, M.; Kapitunova, A.; Galieva, A.; Sukhikh, S.; Astakhova, L.; Antipov, S.; et al. Green Synthesis of Co-Zn Spinel Ferrite Nanoparticles: Magnetic and Intrinsic Antimicrobial Properties. *Materials* **2020**, *13*, 5014. [CrossRef]
25. Muscas, G.; Jovanović, S.; Vukomanović, M.; Spreitzer, M.; Peddis, D. Zn-doped cobalt ferrite: Tuning the interactions by chemical composition. *J. Alloys Compd.* **2019**, *796*, 203–209. [CrossRef]
26. Pullar, R.C. Hexagonal ferrites: A review of the synthesis, properties and applications of hexaferrite ceramics. *Prog. Mater. Sci.* **2012**, *57*, 1191–1334. [CrossRef]
27. Eikeland, A.Z.; Stingaciu, M.; Mamakhel, A.H.; Saura-Múzquiz, M.; Christensen, M. Enhancement of magnetic properties through morphology control of $SrFe_{12}O_{19}$ nanocrystallites. *Sci. Rep.* **2018**, *8*, 7325. [CrossRef] [PubMed]
28. Maltoni, P.; Sarkar, T.; Barucca, G.; Varvaro, G.; Locardi, F.; Peddis, D.; Mathieu, R. Tuning the magnetic properties of hard-soft $SrFe_{12}O_{19}/CoFe_2O_4$ nanostructures via composition/interphase coupling. *J. Phys. Chem. C* **2021**, *125*, 5927–5936. [CrossRef]
29. Cannas, C.; Falqui, A.; Musinu, A.; Peddis, D.; Piccaluga, G. $CoFe_2O_4$ nanocrystalline powders prepared by citrate-gel methods: Synthesis, structure and magnetic properties. *J. Nanopart. Res.* **2006**, *8*, 255–267. [CrossRef]
30. Stingaciu, M.; Topole, M.; McGuiness, P.; Christensen, M. Magnetic properties of ball-milled $SrFe_{12}O_{19}$ particles consolidated by Spark-Plasma Sintering. *Sci. Rep.* **2015**, *5*, 14112. [CrossRef]
31. Batlle, X.; Pérez, N.; Guardia, P.; Iglesias, O.; Labarta, A.; Bartolomé, F.; Garca, L.M.; Bartolomé, J.; Roca, A.G.; Morales, M.P.; et al. Magnetic nanoparticles with bulklike properties (invited). *J. Appl. Phys.* **2011**, *109*, 07B524. [CrossRef]
32. Omelyanchik, A.; da Silva, F.G.; Gomide, G.; Kozenkov, I.; Depeyrot, J.; Aquino, R.; Campos, A.F.C.; Fiorani, D.; Peddis, D.; Rodionova, V.; et al. Effect of citric acid on the morpho-structural and magnetic properties of ultrasmall iron oxide nanoparticles. *J. Alloys Compd.* **2021**, *883*, 160779. [CrossRef]
33. Ribeiro, C.; Costa, C.M.; Correia, D.M.; Nunes-Pereira, J.; Oliveira, J.; Martins, P.; Gonçalves, R.; Cardoso, V.F.; Lanceros-Méndez, S. Electroactive poly(vinylidene fluoride)-based structures for advanced applications. *Nat. Protoc.* **2018**, *13*, 681–704. [CrossRef]
34. Omelyanchik, A.; Antipova, V.; Gritsenko, C.; Kolesnikova, V.; Murzin, D.; Han, Y.; Turutin, A.V.; Kubasov, I.V.; Kislyuk, A.M.; Ilina, T.S.; et al. Boosting Magnetoelectric Effect in Polymer-Based Nanocomposites. *Nanomaterials* **2021**, *11*, 1154. [CrossRef]
35. Morrish, A.H. *The Physical Principles of Magnetism*; IEEE Press: Piscataway, NJ, USA, 1965; Volume 1, ISBN 0-7803-6029-X.
36. Stoner, E.C.; Wohlfarth, E.P. A Mechanism of Magnetic Hysteresis in Heterogeneous Alloys. *Philos. Trans. R. Soc. A Math. Phys. Eng. Sci.* **1948**, *240*, 599–642. [CrossRef]
37. Khatri, B.; Lappe, K.; Noetzel, D.; Pursche, K.; Hanemann, T. A 3D-Printable Polymer-Metal Soft-Magnetic Functional Composite—Development and Characterization. *Materials* **2018**, *11*, 189. [CrossRef] [PubMed]
38. Díaz-García, Á.; Law, J.Y.; Cota, A.; Bellido-Correa, A.; Ramírez-Rico, J.; Schäfer, R.; Franco, V. Novel procedure for laboratory scale production of composite functional filaments for additive manufacturing. *Mater. Today Commun.* **2020**, *24*, 101049. [CrossRef]
39. Díaz-García, Á.; Law, J.Y.; Felix, M.; Guerrero, A.; Franco, V. Functional, thermal and rheological properties of polymer-based magnetic composite filaments for additive manufacturing. *Mater. Des.* **2022**, *219*, 110806. [CrossRef]
40. Takashimizu, Y.; Iiyoshi, M. New parameter of roundness R: Circularity corrected by aspect ratio. *Prog. Earth Planet. Sci.* **2016**, *3*, 2. [CrossRef]
41. Schneider, C.A.; Rasband, W.S.; Eliceiri, K.W. NIH Image to ImageJ: 25 years of image analysis. *Nat. Methods* **2012**, *9*, 671–675. [CrossRef]
42. Roy, M.; Tran, P.; Dickens, T.; Schrand, A. Composite Reinforcement Architectures: A Review of Field-Assisted Additive Manufacturing for Polymers. *J. Compos. Sci.* **2019**, *4*, 1. [CrossRef]